NASA-TP–20210023569

A Guide to Forced Oscillation Data Processing and Analysis

Dan D. Vicroy
Adaptive Aerospace Group, Inc., Hampton, Virginia

June 2023

NASA STI Program Report Series

Since its founding, NASA has been dedicated to the advancement of aeronautics and space science. The NASA scientific and technical information (STI) program plays a key part in helping NASA maintain this important role.

The NASA STI program operates under the auspices of the Agency Chief Information Officer. It collects, organizes, provides for archiving, and disseminates NASA's STI. The NASA STI program provides access to the NTRS Registered and its public interface, the NASA Technical Reports Server, thus providing one of the largest collections of aeronautical and space science STI in the world. Results are published in both non-NASA channels and by NASA in the NASA STI Report Series, which includes the following report types:

- TECHNICAL PUBLICATION. Reports of completed research or a major significant phase of research that present the results of NASA Programs and include extensive data or theoretical analysis. Includes compilations of significant scientific and technical data and information deemed to be of continuing reference value. NASA counterpart of peer-reviewed formal professional papers but has less stringent limitations on manuscript length and extent of graphic presentations.

- TECHNICAL MEMORANDUM. Scientific and technical findings that are preliminary or of specialized interest, e.g., quick release reports, working papers, and bibliographies that contain minimal annotation. Does not contain extensive analysis.

- CONTRACTOR REPORT. Scientific and technical findings by NASA-sponsored contractors and grantees.

- CONFERENCE PUBLICATION. Collected papers from scientific and technical conferences, symposia, seminars, or other meetings sponsored or co-sponsored by NASA.

- SPECIAL PUBLICATION. Scientific, technical, or historical information from NASA programs, projects, and missions, often concerned with subjects having substantial public interest.

- TECHNICAL TRANSLATION. English-language translations of foreign scientific and technical material pertinent to NASA's mission.

Specialized services also include organizing and publishing research results, distributing specialized research announcements and feeds, providing information desk and personal search support, and enabling data exchange services.

For more information about the NASA STI program, see the following:

- Access the NASA STI program home page at http://www.sti.nasa.gov

- Help desk contact information:

https://www.sti.nasa.gov/sti-contact-form/
and select the "General" help request type.

NASA-TP–20210023569

A Guide to Forced Oscillation Data Processing and Analysis

Dan D. Vicroy
Adaptive Aerospace Group, Inc., Hampton, Virginia

National Aeronautics and
Space Administration

Langley Research Center
Hampton, Virginia 23681-2199

June 2023

Available from:

NASA STI Program / Mail Stop 148
NASA Langley Research Center
Hampton, VA 23681-2199
Fax: 757-864-6500

A Guide to Forced Oscillation Data Processing and Analysis

Table of Contents

Abstract

The NASA Langley Research Center Flight Dynamics Branch has a long history of experimental testing of aircraft and spacecraft flight dynamics. One of the frequently used wind tunnel test methods is forced oscillation testing. This method involves a model mounted on a specialized dynamic test rig in a tunnel and oscillated about a body axis, typically at a fixed sinusoidal frequency and amplitude. This report provides the derivation of two commonly used data reduction methods and introduces one new method to extract the linear dynamic derivatives from forced oscillation wind tunnel data.

Introduction

The NASA Langley Research Center Flight Dynamics Branch has a long history of experimental testing of aircraft and spacecraft flight dynamics. One of the frequently used wind tunnel test methods is forced oscillation testing. This method involves a model mounted on a specialized dynamic test rig in a tunnel and oscillated about a body axis, typically at a fixed sinusoidal frequency and amplitude. Figure 1 shows an example of a forced oscillation test setup in the NASA Langley 14- by 22-Foot Subsonic Tunnel for rotation about each body axis. This test rig uses a variable frequency motor to drive a flywheel and bellcrank assembly that can be adjusted to vary the amplitude of the oscillation. The nominal angle of attack is set by rotating the wind tunnel turntable that the oscillation rig is mounted to. This is just one example of a forced oscillation test rig setup. Other rigs may use different methods to change angles, frequencies of amplitudes. Some of the newer dynamic test rigs are capable of variable frequency and amplitude motions such as Schroeder sweeps or replicating flight maneuvers. The analysis of these types of motions are outside the scope of this report.

The fixed sinusoidal frequency and amplitude test method has existed for many years. References 1 thru 19 provide some examples of forced-oscillation test results. The data processing and analysis used for this test technique has evolved without much supporting documentation. The purpose of this report is to provide some background into this evolution along with a derivation of the current data reduction methods, as well as a discussion of their practical application and considerations and as an archival reference for future researchers.

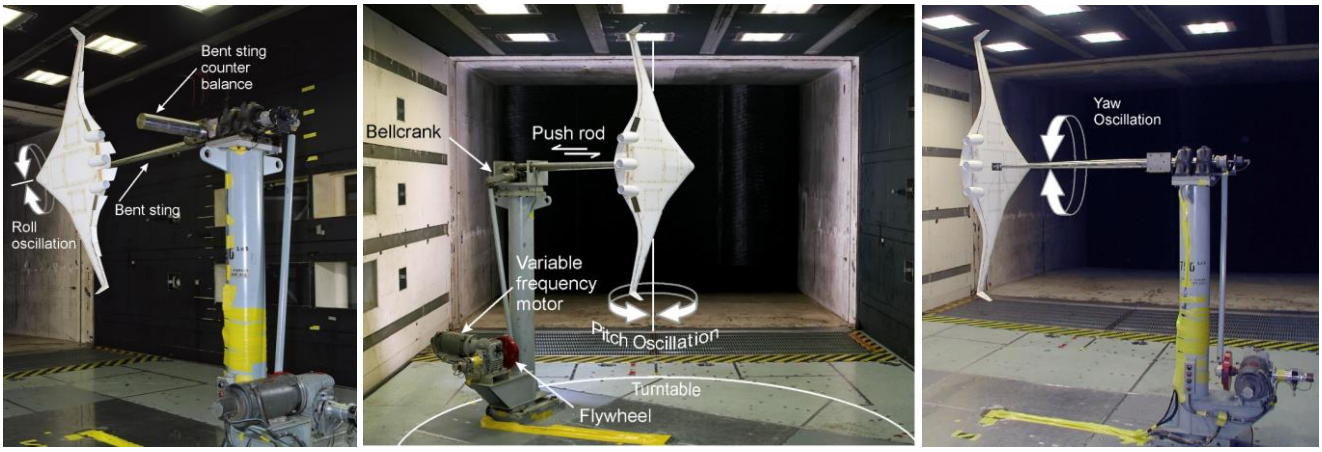

(a) Roll oscillation (b) Pitch oscillation (c) Yaw oscillation

Figure 1 – Forced oscillation test setup.

Background

The history of aircraft stability analysis extends to the very beginning of human flight. Hultberg provides a nice review of the early work, including a history of dynamic test techniques, in the appendix of his 1998 paper (ref. 20). The very first NACA technical report focused on aircraft stability. NACA Report #1, Part I by J.C. Hunsaker, was entitled "Experimental Analysis of Inherent Longitudinal Stability for a Typical Biplane" (ref. 21). Much of this early stability analysis used small perturbation theory to derive stability equations. This approach introduced the dynamic damping and rotary coefficients to model the airplane motions. The rotary and forced oscillation testing techniques were developed to determine these coefficients. The focus of this report is the data reduction methods developed for the forced oscillation testing. There are three methods that will be examined: the "Integration Method," the "Specific Point Method" and the "Multi-point Method."

The Specific Point method for deriving the dynamic derivatives from sinusoidal forced oscillation data has a long, although somewhat obscure, history. Hultberg credits the first introduction of this forced-oscillation data reduction technique to Bird, Jaquet and Cowan in 1951 (ref. 1). Campbell, Johnson, and Hewes also tried this method and compared against the more traditional Integration Method to process forced-oscillation data (ref. 2). This method however proved somewhat cumbersome for the measurement and data processing tools available at that time. The Integration Method, which is described by Chambers and Grafton, proved to be easier to implement with the analog data systems of that time and was the preferred method by NASA for many years (ref. 3). The proliferation of digital computing in the 1980's along with an emphasis on high-angle-of-attack aircraft maneuverability in the 1990's provided a renewed interest in dynamic testing and data processing techniques. Hultberg compares the Specific Point method with the Integration Method in his 1998 paper (ref. 20). Brandon and Foster provided a similar comparison in which they referred to the data reduction technique as the "Single Point Method." (ref. 12). The term "Crossing Points Method" is perhaps a better description of this method as the technique utilizes multiple crossing point locations in the oscillation cycle. The derivation of these two methods along with a proposed new Multi-point Method will be examined in the following sections.

Symbols and Nomenclature

A	oscillation amplitude, deg
b	span, ft
C_m	pitching moment coefficient, $\frac{M_a}{\bar{q}S\bar{c}}$
C_{m_o}	nominal pitching moment coefficient
C_{m_q}	$\partial C_m/\partial\left(\frac{q\bar{c}}{2V}\right)$
$C_{m_{\dot{q}}}$	$\partial C_m/\partial\left(\frac{\dot{q}\bar{c}^2}{4V^2}\right)$
C_{m_α}	$\frac{\partial C_m}{\partial \alpha}$
$C_{m_{\dot{\alpha}}}$	$\partial C_m/\partial\left(\frac{\dot{\alpha}\bar{c}}{2V}\right)$
$\bar{c}$	mean aerodynamic chord, ft
g_m	gradient of standard deviation
M_a	aerodynamic pitching moment, ft-lb
M_b	balance measured pitching moment, ft-lb
M_i	inertial pitching moment, ft-lb
n	integer index
n_{cyc}	number of cycles
p	roll rate about X body axis, deg/s
q	pitch rate about Y body axis, deg/s

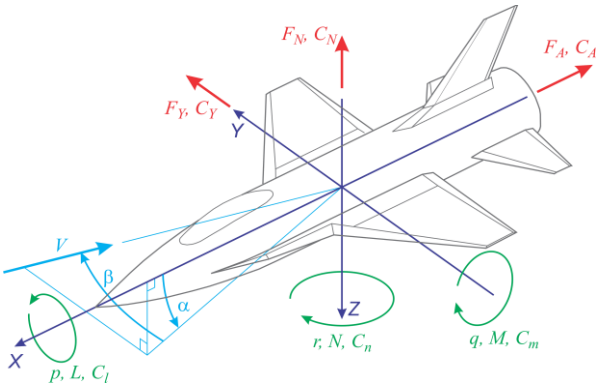

Figure 2 - Axes with force and moment orientation.

$\bar{q}$	tunnel dynamic pressure, lb/ft^2
R^2	coefficient of determination
r	yaw rate about Z body axis, deg/s
S	reference area, ft^2
SS_r	sum of squares of the residual
SS_T	total sum of squares
T	period of multiple complete cycles, sec
t	time, sec

$\acute{t}$	selected time, sec
t_o	start time, sec
V	tunnel velocity, ft/s
α	angle of attack, deg
α_o	nominal angle of attack of oscillation, deg
β	sideslip angle, deg
β_o	nominal sideslip angle of oscillation, deg
σ	standard deviation
θ	pitch angle, deg
$\acute{\theta}$	selected pitch angle, deg
θ_0	nominal pitch angle of oscillation, deg
ω	frequency, s^{-1}

Subscript

max	maximum value
min	minimum value

Superscript

+	positive rate value
-	negative rate value
$\cdot$	$\frac{d}{dt}$
$\cdot\cdot$	$\frac{d^2}{dt^2}$

Forced Oscillation Dynamic Derivative Methods

The following sections will show the derivation of three methods used to compute dynamic derivative coefficient values from sinusoidal forced oscillation wind tunnel data. The derivations will focus on the pitching moment coefficients derived from pitch oscillations. However, the same approach applies to the other dynamic force and moment coefficients and oscillations about the roll and yaw axes. A complete set of dynamic force and moment coefficient equations are provided in the Appendix. Also included in the appendix is a step-by-step description of the implemented data processing approach for the Specific Point method.

Linear Dynamic Derivative Model

Sinusoidal forced-motion wind tunnel testing is characterized by the tunnel velocity *(V)* or dynamic pressure *($\bar{q}$)*, and the amplitude *(A)* and frequency *(ω)* of the oscillation about a nominal attitude angle *(θ_0)*. For example, sinusoidal oscillation in pitch *(θ)* is:

$$\theta(t) = \theta_0 + A\ sin(\omega t) = \alpha(t) \tag{1}$$

Where:

θ_0	=	nominal pitch angle about which the oscillation occurs
t	=	time
α	=	angle of attack

The pitch rate (q) and pitch acceleration ($\dot{q}$) are the first and second derivative of the pitch angle with respect to time.

$$\dot{\theta}(t) = A\omega\ cos(\omega t) = \dot{\alpha}(t) = q(t) \tag{2}$$

$$\ddot{\theta}(t) = -A\omega^2\ sin(\omega t) = \ddot{\alpha}(t) = \dot{q}\,(t) \tag{3}$$

The balance measured pitching moment *(M_b)* during the oscillation is the sum of the inertial *(M_i)* and aerodynamic *(M_a)* components.

$$M_b(t) = M_i(t) + M_a(t) \tag{4}$$

$$M_b(t) = M_i(t) + \bar{q}S\bar{c}C_m(t) \tag{5}$$

The pitching moment coefficient (C_m) about a nominal angle of attack (α_o) is often expressed in a linear first-order Taylor Series expansion as:

$$C_m(\alpha_o) = C_{m_o}(\alpha_o) + C_{m_\alpha}(\alpha_o)\Delta\alpha(t) + \frac{\bar{c}q(t)}{2V}C_{m_q}(\alpha_o) + \frac{\bar{c}\dot{\alpha}(t)}{2V}C_{m_{\dot{\alpha}}}(\alpha_o) + \left(\frac{\bar{c}}{2V}\right)^2 \dot{q}(t)C_{m_{\dot{q}}}(\alpha_o) \tag{6}$$

This linear model assumes that the coefficient values (C_{m_o}, C_{m_α}, C_{m_q}, $C_{m_{\dot{\alpha}}}$, and $C_{m_{\dot{q}}}$) are constant over the oscillation cycle. Subtracting the wind-off tare measurements from the wind-on balance measurements removes the inertial and still-air damping values yielding the desired aerodynamic effects.

$$M_b(t) - M_i(t) =$$

$$\bar{q}S\bar{c}\left[C_{m_o}(\alpha_o) + C_{m_\alpha}(\alpha_o)\Delta\alpha(t) + \frac{\bar{c}q(t)}{2V}C_{m_q}(\alpha_o) + \frac{\bar{c}\dot{\alpha}(t)}{2V}C_{m_{\dot{\alpha}}}(\alpha_o) + \left(\frac{\bar{c}}{2V}\right)^2 \dot{q}(t)C_{m_{\dot{q}}}(\alpha_o)\right] \tag{7}$$

Substituting equations 2 and 3 for $\dot{\alpha}(t)$, $q(t)$, and $\dot{q}(t)$, and $A\sin(\omega t)$ for $\Delta\alpha(t)$ yields:

$$M_b(t) - M_i(t) =$$

$$= \bar{q}S\bar{c}\left\{C_{m_o}(\alpha_o) + A\sin(\omega t)\left[C_{m_\alpha}(\alpha_o) - \left(\frac{\bar{c}\omega}{2V}\right)^2 C_{m_{\dot{q}}}(\alpha_o)\right] + \frac{\bar{c}\omega}{2V}A\cos(\omega t)\left[C_{m_q}(\alpha_o) + C_{m_{\dot{\alpha}}}(\alpha_o)\right]\right\} \tag{8}$$

Equation 8 can be further simplified as:

$$\frac{1}{\bar{q}S\bar{c}}[M_b(t) - M_i(t)] = C_m(\alpha_o) = C_{m_o}(\alpha_o) + A\sin(\omega t)\,\overline{C_{m_\alpha}}(\alpha_o) + \frac{\bar{c}\omega}{2V}A\cos(\omega t)\,\overline{C_{m_q}}(\alpha_o) \tag{9}$$

Where the in-phase term ($\overline{C_{m_\alpha}}$) is:

$$\overline{C_{m_\alpha}}(\alpha_o) = C_{m_\alpha}(\alpha_o) - \left(\frac{\bar{c}\omega}{2V}\right)^2 C_{m_{\dot{q}}}(\alpha_o) \tag{10}$$

and the out-of-phase term ($\overline{C_{m_q}}$) is:

$$\overline{C_{m_q}}(\alpha_o) = C_{m_q}(\alpha_o) + C_{m_{\dot{\alpha}}}(\alpha_o) \tag{11}$$

Recall that the underlying assumption is that the coefficient values$\left(C_{m_o}, \overline{C_{m_\alpha}} \text{ and } \overline{C_{m_q}}\right)$ are constant over the oscillation cycle. The oscillation amplitude must therefore be sufficiently small for this approximation to hold. However, the oscillation amplitude must also be sufficiently large to provide enough signal-to-noise ratio to discern the difference between the wind-on balance measurements and the wind-off tare measurements. This trade between minimal oscillation amplitude and signal-to-noise is highly dependent on the model mass properties, the model geometry, the balance range and resolution, and the test

conditions. This trade is generally done ad hoc, using engineering judgement and thus a potential source of error or increased uncertainty.

As discussed earlier, there have historically been two different methods used to extract the linear coefficients, C_{m_o} , $\overline{C_{m_\alpha}}$, and $\overline{C_{m_q}}$ of equation 9 from the balance measurements. The derivations of the Integration and Specific Point methods are described in the following sections.

Integration Method

As the name implies the Integration Method integrates the balance measurements over several complete oscillation cycles to derive the coefficient values. From equation 9 it can be observed that the C_{m_o} value is the mean value about which the in-phase $\overline{C_{m_\alpha}}$ and an out-of-phase $\overline{C_{m_q}}$ components oscillate. This mean value can be found by integrating the difference in the balance wind-on and wind-off measurements over a period (T) of several complete cycles, divided by that period.

$$C_{m_0}(\alpha_o) = \frac{1}{\bar{q}S\bar{c}T}\int_{t_0}^{t_0+T}[M_b(t) - M_i(t)]\,dt \tag{12}$$

where:

$$T = \frac{2\pi n_{cyc}}{\omega},\ n_{cyc} = 1, 2, 3, \cdots \text{ number of cycles} \tag{13}$$

The in-phase term ($\overline{C_{m_\alpha}}$) can be derived by multiplying equation 9 by $\frac{2}{AT}\sin(\omega t)$ and then integrating over the measurement period.

$$\begin{aligned}\frac{2}{\bar{q}S\bar{c}AT}\int_{t_0}^{t_0+T}[M_b(t) - M_i(t)]\sin(\omega t)\,dt \quad &= \frac{2}{AT}C_{m_0}\int_{t_0}^{t_0+T}\sin(\omega t)\,dt \\ &+ \frac{2}{T}\overline{C_{m_\alpha}}\int_{t_0}^{t_0+T}\sin^2(\omega t)\,dt \\ &+ \frac{\bar{c}\omega}{TV}\,\overline{C_{m_q}}\int_{t_0}^{t_0+T}\sin(\omega t)\cos(\omega t)\,dt\end{aligned} \tag{14}$$

$$\begin{aligned}\frac{2}{\bar{q}S\bar{c}AT}\int_{t_0}^{t_0+T}[M_b(t) - M_i(t)]\sin(\omega t)\,dt \quad &= \frac{2}{AT}C_{m_0}\frac{-1}{\omega}\cos(\omega t)\Big|_{t_0}^{t_0+T} \\ &+ \frac{2}{T}\overline{C_{m_\alpha}}\left[\frac{t}{2} - \frac{1}{4\omega}\sin(2\omega t)\right]\Big|_{t_0}^{t_0+T} \\ &+ \frac{\bar{c}}{2TV}\,\overline{C_{m_q}}\sin^2(\omega t)\Big|_{t_0}^{t_0+T}\end{aligned} \tag{15}$$

Note that: $$\cos(\omega t)\Big|_{t_0}^{t_0+T} = \sin(2\omega t)\Big|_{t_0}^{t_0+T} = \sin^2(\omega t)\Big|_{t_0}^{t_0+T} = 0 \tag{16}$$

Therefore: $$\overline{C_{m_\alpha}} = \frac{2}{\bar{q}S\bar{c}AT}\int_{t_0}^{t_0+T}[M_b(t) - M_i(t)]\sin(\omega t)\,dt \tag{17}$$

The out-of-phase damping term ($\overline{C_{m_q}}$) can be derived in a similar fashion by multiplying equation 9 by $\frac{4V}{\bar{c}\omega AT}\cos(\omega t)$ and integrating over the measurement period.

$$\frac{4V}{\bar{q}S\bar{c}^2\omega AT}\int_{t_0}^{t_0+T}[M_b(t)-M_i(t)]\cos(\omega t)\,dt = \frac{4V}{\bar{c}\omega AT}C_{m_0}\int_{t_0}^{t_0+T}\cos(\omega t)\,dt + \frac{4V}{\bar{c}\omega T}\overline{C_{m_\alpha}}\int_{t_0}^{t_0+T}\sin(\omega t)\cos(\omega t)\,dt + \frac{2}{T}\overline{C_{m_q}}\int_{t_0}^{t_0+T}\cos^2(\omega t)\,dt \quad (18)$$

$$\frac{4V}{\bar{q}S\bar{c}^2\omega AT}\int_{t_0}^{t_0+T}[M_b(t)-M_i(t)]\cos(\omega t)\,dt = \frac{4V}{\bar{c}\omega AT}C_{m_0}\frac{1}{\omega}\sin(\omega t)\Big|_{t_0}^{t_0+T} + \frac{2V}{\bar{c}\omega^2 T}\overline{C_{m_\alpha}}\sin^2(\omega t)\Big|_{t_0}^{t_0+T} + \frac{2}{T}\overline{C_{m_q}}\left[\frac{t}{2}+\frac{1}{4\omega}\sin(2\omega t)\right]\Big|_{t_0}^{t_0+T} \quad (19)$$

Since: $$\sin(\omega t)\Big|_{t_0}^{t_0+T} = \sin(2\omega t)\Big|_{t_0}^{t_0+T} = \sin^2(\omega t)\Big|_{t_0}^{t_0+T} = 0 \quad (20)$$

$$\overline{C_{m_q}} = \frac{4V}{\bar{q}S\bar{c}^2\omega AT}\int_{t_0}^{t_0+T}[M_b(t)-M_i(t)]\cos(\omega t)\,dt \quad (21)$$

Note that the integration intervals for all three parameters (C_{m_0}, $\overline{C_{m_\alpha}}$, and $\overline{C_{m_q}}$) are over complete cycles (t_0 to t_0+T). The forced oscillation time history data must be trimmed to complete cycle intervals prior to integrating or errors will be introduced, since the integrated terms that reduce to zero over complete intervals are non-zero over partial intervals.

As noted in the Background section, the Integration Method was easier to implement back when the data systems were analog. The analog implementation merely required the averaging of the in-phase and out-of-phase balance voltages (ref. 3). With digital data systems this is no longer any advantage. This method also has some inherent limitations which will be highlighted later in the report.

Specific Point Method

The derivation of the Specific Point Method begins with the difference between the wind-on and wind-off balance measurements of equation 8, repeated below.

$$M_b(t)-M_i(t) = \bar{q}S\bar{c}\left\{C_{m_o}(\alpha_o) + A\,sin(\omega t)\left[C_{m_\alpha}(\alpha_o) - \left(\frac{\bar{c}\omega}{2V}\right)^2 C_{m_{\dot{q}}}(\alpha_o)\right] + \frac{\bar{c}\omega}{2V}A\,cos(\omega t)\left[C_{m_q}(\alpha_o)+C_{m_{\dot{\alpha}}}(\alpha_o)\right]\right\} \quad (8)$$

Recall from equations 2 and 3 that the maximum angular rate and zero angular acceleration occur when $\cos(\omega t)=1$ and $\sin(\omega t)=0$, which corresponds to the beginning and ending of each oscillation cycle when:

$$t = \frac{2n\pi}{\omega}, n = 0,1,2,3,\ldots \quad (22)$$

Note that this analysis is excluding any transients that may occur during the test rig startup or stopping. Extracting the measurements at the zero angular acceleration points yields values at the maximum angular rate values.

$$M_b\left(\frac{2n\pi}{\omega}\right) - M_i\left(\frac{2n\pi}{\omega}\right) = M_b(q_{max}) - M_i(q_{max}) = \bar{q}S\bar{c}\left\{C_{m_o}(\alpha_o) + \frac{\bar{c}A\omega}{2V}\left[C_{m_q}(\alpha_o) + C_{m_{\dot{\alpha}}}(\alpha_o)\right]\right\} \quad (23)$$

The minimum angular rate occurs when $\cos(\omega t) = -1$, corresponding to the mid-cycle crossing point when:

$$t = \frac{(2n+1)\pi}{\omega}, n = 0,1,2,3,\ldots \quad (24)$$

Extracting the measurements at these zero angular acceleration points yields values at the minimum angular rate.

$$\begin{aligned} M_b\left(\frac{(2n+1)\pi}{\omega}\right) - M_i\left(\frac{(2n+1)\pi}{\omega}\right) &= M_b(q_{min}) - M_i(q_{min}) \\ &= \bar{q}S\bar{c}\left\{C_{m_o}(\alpha_o) - \frac{\bar{c}A\omega}{2V}\left[C_{m_q}(\alpha_o) + C_{m_{\dot{\alpha}}}(\alpha_o)\right]\right\} \end{aligned} \quad (25)$$

Taking the difference between the measurements at the maximum (eq. 23) and minimum rates (eq. 25) yields:

$$\begin{aligned} M_b(q_{max}) - M_i(q_{max}) - M_b(q_{min}) + M_i(q_{min}) &= \bar{q}S\bar{c}\left\{\frac{\bar{c}A\omega}{V}\left[C_{m_q}(\alpha_o) + C_{m_{\dot{\alpha}}}(\alpha_o)\right]\right\} \\ &= \bar{q}S\bar{c}\left\{\frac{\bar{c}A\omega}{V}\left[\overline{C_{m_q}}(\alpha_o)\right]\right\} \end{aligned} \quad (26)$$

Solving for $\overline{C_{m_q}}(\alpha_o)$ yields:

$$\begin{aligned} \overline{C_{m_q}}(\alpha_o) &= \frac{V}{\bar{c}A\omega}\left[\frac{M_b(q_{max}) - M_i(q_{max}) - M_b(q_{min}) + M_i(q_{min})}{\bar{q}S\bar{c}}\right] \\ &= \frac{V}{\bar{c}A\omega}\left[C_m(q_{max}) - C_m(q_{min})\right] \end{aligned} \quad (27)$$

Taking the sum of the measurements at the maximum and minimum rates yields:

$$M_b(q_{max}) - M_i(q_{max}) + M_b(q_{min}) - M_i(q_{min}) = \bar{q}S\bar{c}\left[2C_{m_o}(\alpha_o)\right] \quad (28)$$

Solving for $C_{m_o}(\alpha_o)$ yields:

$$C_{m_o}(\alpha_o) = \frac{1}{2}\left(\frac{M_b(q_{max}) - M_i(q_{max}) + M_b(q_{min}) - M_i(q_{min})}{\bar{q}S\bar{c}}\right) = \frac{1}{2}\left[C_m(q_{max}) + C_m(q_{min})\right] \quad (29)$$

The $\overline{C_{m_\alpha}}(\alpha_o)$ term can be determined in a similar manner by taking the difference of the balance measurements at the maximum and minimum angular acceleration points. The maximum angular acceleration occurs when $\sin(\omega t) = -1$ or:

$$t = \frac{(4n+3)\pi}{2\omega}, n = 0,1,2,3,\ldots \quad (30)$$

$$\begin{aligned} M_b\left(\frac{(4n+3)\pi}{2\omega}\right) - M_i\left(\frac{(4n+3)\pi}{2\omega}\right) &= M_b(\dot{q}_{max}) - M_i(\dot{q}_{max}) \\ &= \bar{q}S\bar{c}\left\{C_{m_o}(\alpha_o) - A\left[C_{m_\alpha}(\alpha_o) - \left(\frac{\bar{c}\omega}{2V}\right)^2 C_{m_{\dot{q}}}(\alpha_o)\right]\right\} \end{aligned} \quad (31)$$

The minimum angular acceleration occurs when:

$$t = \frac{(4n+1)\pi}{2\omega}, n = 0,1,2,3, \ldots \tag{32}$$

$$\begin{aligned} M_b\left(\frac{(4n+1)\pi}{2\omega}\right) - M_i\left(\frac{(4n+1)\pi}{2\omega}\right) &= M_b(\dot{q}_{min}) - M_i(\dot{q}_{min}) \\ &= \bar{q}S\bar{c}\left\{C_{m_o}(\alpha_o) + A\left[C_{m_\alpha}(\alpha_o) - \left(\frac{\bar{c}\omega}{2V}\right)^2 C_{m_{\dot{q}}}(\alpha_o)\right]\right\} \end{aligned} \tag{33}$$

Taking the difference between the measurements at the maximum and minimum angular acceleration yields:

$$\begin{aligned} M_b(\dot{q}_{max}) - M_i(\dot{q}_{max}) - M_b(\dot{q}_{min}) + M_i(\dot{q}_{min}) &= -2A\bar{q}S\bar{c}\left[C_{m_\alpha}(\alpha_o) - \left(\frac{\bar{c}\omega}{2V}\right)^2 C_{m_{\dot{q}}}(\alpha_o)\right] \\ &= -2A\bar{q}S\bar{c}\left[\overline{C_{m_\alpha}}(\alpha_o)\right] \end{aligned} \tag{34}$$

Solving for $\overline{C_{m_\alpha}}(\alpha_o)$ yields:

$$\begin{aligned} \overline{C_{m_\alpha}}(\alpha_o) &= \frac{-1}{2A}\left[\frac{M_b(\dot{q}_{max}) - M_i(\dot{q}_{max}) - M_b(\dot{q}_{min}) + M_i(\dot{q}_{min})}{\bar{q}S\bar{c}}\right] \\ &= \frac{-1}{2A}\left[C_m(\dot{q}_{max}) - C_m(\dot{q}_{min})\right] \end{aligned} \tag{35}$$

Note that the only required wind-off and wind-on measurements are at the angular rate and acceleration maximum and minimum points. The other data points in the oscillation cycle are not used.

One of the byproducts of the Specific Point method is the ability to estimate the standard deviation of the measured dynamic coefficient values using general uncertainty analysis (ref. 22). For each oscillation cycle there will be a pair of minimum and maximum rate and acceleration measurements. The mean and standard deviation of these measurements can be computed based on the number of measured oscillation cycles. These values are used to estimate the standard deviation of the dynamic coefficient values.

Applying the general uncertainty analysis to equation 27 for $\overline{C_{m_q}}$ and assuming the amplitude (*A*) and frequency (ω) are constants and the standard deviation of the tare values are negligible, yields:

$$\sigma^2_{\overline{C_{m_q}}} = \left(\frac{\partial \overline{C_{m_q}}}{\partial V}\right)^2 \sigma^2_V + \left(\frac{\partial \overline{C_{m_q}}}{\partial C_{m_{q_{max}}}}\right)^2 \sigma^2_{C_{m_{q_{max}}}} + \left(\frac{\partial \overline{C_{m_q}}}{\partial C_{m_{q_{min}}}}\right)^2 \sigma^2_{C_{m_{q_{min}}}} \tag{36}$$

where:

$$\frac{\partial \overline{C_{m_q}}}{\partial V} = \frac{1}{\bar{c}A\omega}\left(C_{m_{q_{max}}} - C_{m_{q_{min}}}\right) \tag{37}$$

$$\frac{\partial \overline{C_{m_q}}}{\partial C_{m_{q_{max}}}} = \frac{V}{\bar{c}A\omega} \tag{38}$$

$$\frac{\partial \overline{C_{m_q}}}{\partial C_{m_{q_{min}}}} = \frac{-V}{\bar{c}A\omega} \tag{39}$$

Therefore:

$$\sigma^2_{\overline{C_{mq}}} = \left[\frac{1}{\bar{c}A\omega}\left(C_{m_{q_{max}}} - C_{m_{q_{min}}}\right)\right]^2 \sigma^2{}_V + \left(\frac{V}{\bar{c}A\omega}\right)^2 \left[\sigma^2{}_{C_{mq_{max}}} + \sigma^2{}_{C_{mq_{min}}}\right] \tag{40}$$

or

$$\sigma_{\overline{C_{mq}}} = \frac{1}{\bar{c}A\omega}\left\{\left(C_{m_{q_{max}}} - C_{m_{q_{min}}}\right)^2 \sigma^2{}_V + V^2\left[\sigma^2{}_{C_{mq_{max}}} + \sigma^2{}_{C_{mq_{min}}}\right]\right\}^{\frac{1}{2}} \tag{41}$$

Characteristics and Limitations of Linear Dynamic Derivative Model

As aircraft have become more maneuverable and have expanded flight envelopes into higher angle of attack and sideslip regions, the limitations of a linear dynamic derivative model have become more apparent. This can be illustrated by comparing model and measured data at linear and non-linear angle of attack regions. Figure 3 shows the idealized linear model hysteresis loop of the dynamic pitching moment coefficient of equation 9 about a nominal pitch angle (θ_0), with an oscillation amplitude (A) and positive values for C_{m_0}, $\overline{C_{m_\alpha}}$ and $\overline{C_{m_q}}$. Also shown are the maximum and minimum pitch rate and acceleration points used in the Specific Point method described in the previous section. The magnitude of the $\overline{C_{m_q}}$ value determines the vertical thickness of the linear model hysteresis loop and the sign dictates the direction of the loop (positive is clockwise and negative is counterclockwise). The $\overline{C_{m_\alpha}}$ term specifies the tilt or slope of the loop which will be negative for stable aircraft.

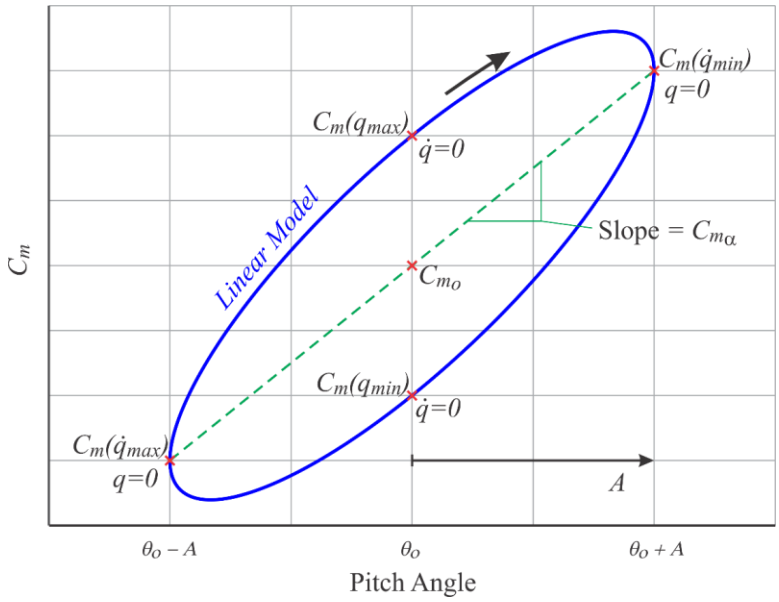

Figure 3 – Linear model hysteresis loop of the dynamic pitching moment coefficient.

Figure 4 shows an example of forced oscillation pitching moment data from a tailless aircraft configuration as reported in reference 17. The figure includes the static pitching moment measurements from an angle of attack sweep along with the pitching moment hysteresis loops from 30 cycles of pitch oscillation at a frequency of 1 Hz and amplitude of 5 degrees. Also shown in the figure are arrows indicating the direction of the oscillation. The oscillation data at the lower 5-degree nominal pitch angle show good

repeatability over the 30 cycles and a similar elliptical shape as the linear dynamic model shown in figure 3. The oscillation data about the higher 15-degree nominal pitch angle shows less repeatability, indicating some flow unsteadiness, and does not resemble the elliptical linear dynamic model shape.

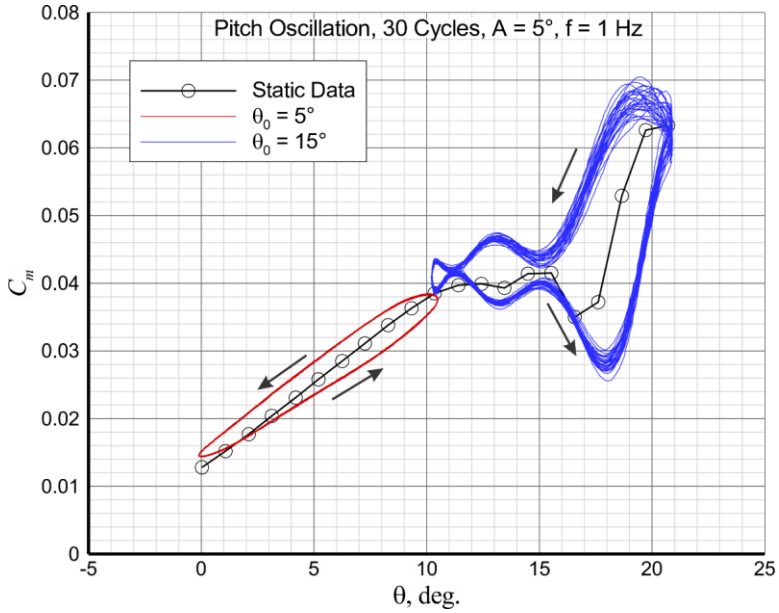

Figure 4 – Pitching moment coefficient static and forced-oscillation hysteresis loop data example (Ref. 17).

A statistical measure of how well the forced oscillation data fits the linear dynamic model can be obtained through the coefficient of determination (R^2). In the case of this pitching moment example the coefficient of determination is computed as:

$$R^2 = 1 - \frac{SS_r}{SS_T} \tag{42}$$

Where SS_r is the sum of squares of the residual between the measured data and the model and SS_T is the total sum of squares of the difference between the measured data and the mean of the measured data.

$$SS_r = \sum_i \left(C_{m_{data\,i}} - C_{m_{model\,i}}\right)^2 \tag{43}$$

$$SS_T = \sum_i \left(C_{m_{data\,i}} - \overline{C_m}\right)^2 \tag{44}$$

$$\overline{C_m} = \frac{1}{n}\sum_i^n C_{m_{data\,i}} \tag{45}$$

Figure 5 shows a comparison of the dynamic linear model hysteresis loops generated from the coefficient values obtained from both the Integral and Specific Point methods. Also shown in the figure are the corresponding coefficient of determination values. The coefficient values from each method are also listed in table 1. Both methods produce similar coefficient values and a good model fit to the lower pitch oscillation data (Fig. 5 a).

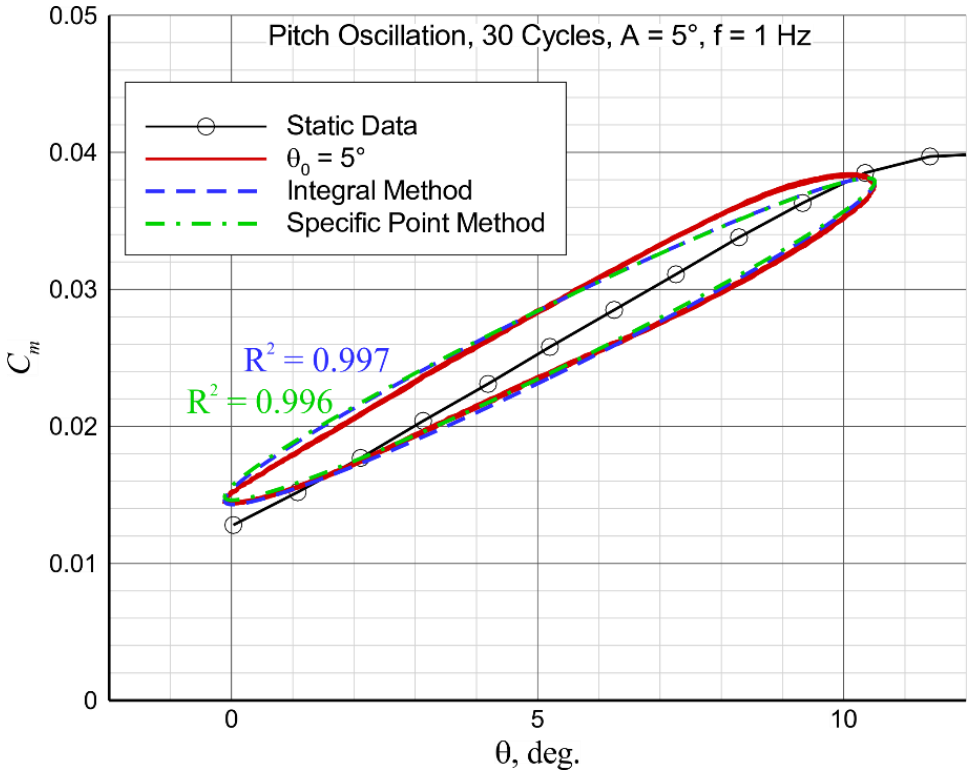

(a) Oscillation about 5° nominal pitch angle.

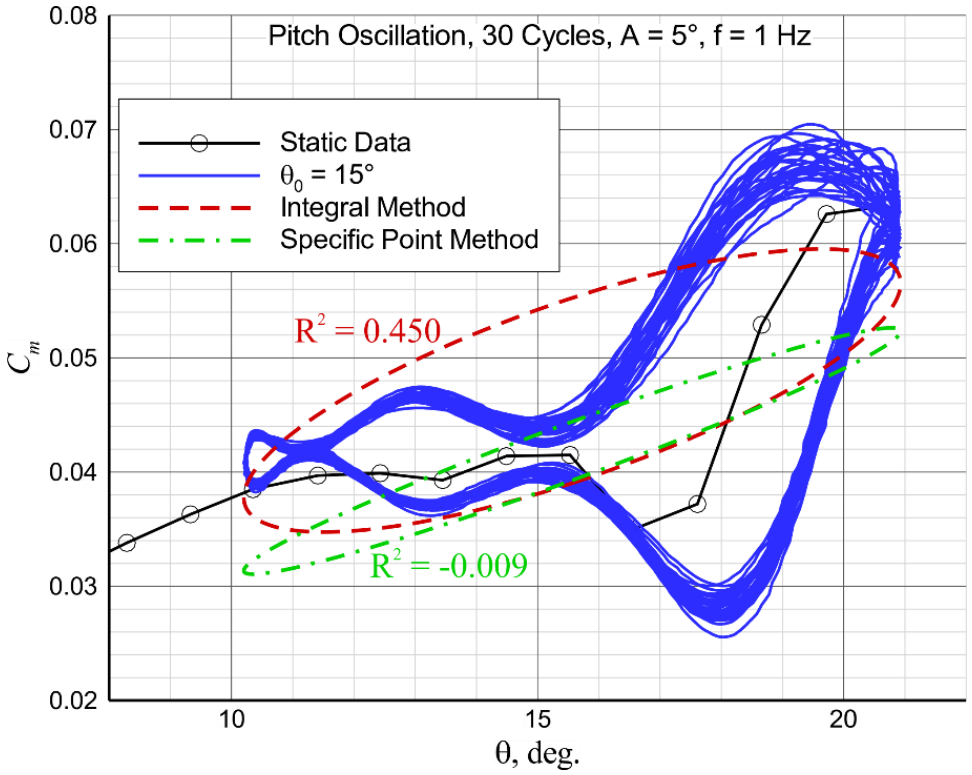

(b) Oscillation about 15° nominal pitch angle

Figure 5 – Linear model hysteresis loop comparison from Integral and Specific Point methods.

Table 1 - Linear dynamic model coefficient values from Integral and Specific Point methods.

Method	$\boldsymbol{\theta_0}$, deg	*Amp*, deg	*f*, Hz	C_{m_0}	$\overline{C_{m_\alpha}}$	$\overline{C_{m_q}}$	R^2	R^2 @ θ_o
Integral	5.2	5.3	1.0	0.0262	0.1252	-0.9478	0.997	0.991
Specific Point				0.0264	0.1239	-0.8919	0.996	0.999
Integral	15.6	5.4	1.0	0.0471	0.1001	-2.8773	0.450	-0.638
Specific Point				0.0418	0.1119	-0.9112	-0.009	0.930

At the higher nominal pitch angle (Fig. 5 b) neither method produces a good fit to the data indicating that the linear dynamic model is not sufficient to capture the dynamics observed over the entire oscillation cycle. The Integral method resulted in a better R^2 value, but the Specific Point method matched the data at the zero pitch acceleration points better. This is an important distinction between the two methods. The Integral method uses all the cycle data to compute the coefficient values that best fit the measurements. It therefore only produces relevant dynamic coefficient values when the measured data resemble the elliptical hysteresis loop of the linear model. The Specific Point method is only using the data at the crossing points and consequently is less dependent on the measured hysteresis data being elliptical. In other words, the Specific Point method is not constrained to the linear coefficient model of equation 9 where the coefficient values are assumed to be constant over the entire oscillation cycle. Another illustration of this is comparing the coefficient of determination (R^2) values of the two methods computed at the nominal pitch angle (θ_o) crossing values. For the linear 5° case there is very little difference in the two methods. For the 15° non-linear case the Specific Point method clearly provides a better match to the observed rate damping at the nominal pitch angle.

The Specific Point method also has the flexibility to provide different damping derivative ($\overline{C_{m_q}}$) values for positive and negative rates or values that are a function of the rates. Hultberg (ref. 20) concludes: "The damping data should not be linearized, but merely associated with the actual nondimensionalized body axis rate. This includes having separate damping values for positive and negative rates. Using this format, damping characteristics in asymmetric conditions such as nonzero sideslip angles or control deflections can be accurately measured." The Specific Point method allows for this modeling flexibility.

Multi-point Method

The Multi-point method is an extension of the Specific Point method. This method is new and has yet to be applied extensively. The Specific Point method only uses the data at the zero rate (q) and zero acceleration ($\dot{q}$) points to compute the $\overline{C_{m_\alpha}}$ and $\overline{C_{m_q}}$ coefficients, respectively, for the nominal pitch angle (θ_o). The remaining off-peak hysteresis loop data are ignored. The Multi-point method is similar to the Specific Point method, but it uses the data from all the pitch angles throughout the oscillation cycle. The Multi-point method applies the linear model of equation 8 at each pitch angle of the oscillation cycle and computes a $\overline{C_{m_q}}$ and $C_{m_{\dot{q}}}$ value for that angle rather than a single value for the entire oscillation cycle. As noted earlier, the linear model assumption used in the Specific Point and Integral methods may not be valid over an oscillation cycle, particularly if the oscillation amplitude is large enough to include non-linear regions. However, the linear model assumption can be valid over sufficiently small angular segments of the oscillation cycle.

Recall the linear Taylor Series pitching moment coefficient model of equation 6:

$$C_m(\alpha_o) = C_{m_o}(\alpha_o) + C_{m_\alpha}(\alpha_o)\Delta\alpha(t) + \frac{\bar{c}q(t)}{2V}C_{m_q}(\alpha_o) + \frac{\bar{c}\dot{\alpha}(t)}{2V}C_{m_{\dot{\alpha}}}(\alpha_o) + \left(\frac{\bar{c}}{2V}\right)^2 \dot{q}(t)C_{m_{\dot{q}}}(\alpha_o) \tag{6}$$

Replacing the C_{m_q} and $C_{m_{\dot{\alpha}}}$ terms with $\overline{C_{m_q}}$ (eq. 10) yields:

$$C_m(\alpha_o) = \underbrace{C_{m_o}(\alpha_o) + C_{m_\alpha}(\alpha_o)\Delta\alpha(t)}_{\text{Static terms}} + \underbrace{\frac{\bar{c}}{2V}q(t)\,\overline{C_{m_q}}\,(\alpha_o) + \left(\frac{\bar{c}}{2V}\right)^2 \dot{q}(t)\,C_{m_{\dot{q}}}\,(\alpha_o)}_{\text{Dynamic terms}} \tag{46}$$

Note that the first two terms of the above equation represent the static aerodynamic contribution and the last two are the dynamic components. The Multi-point method applies the above model to any pitch angle within the oscillation cycle.

At any pitch angle $(\acute{\theta})$within the oscillation cycle there are a pair of pitching moment coefficient values corresponding to negative (q^-) and positive (q^+) pitch rates as shown in figure 6. The pitch rates are of equal magnitude and opposite sign. The only exception is at the maximum and minimum pitch values where the rates are zero.

$$\acute{\theta} = \theta_o + A\sin(\omega\acute{t}) \tag{47}$$

$$\omega\acute{t} = \sin^{-1}\left(\frac{\acute{\theta}-\theta_o}{A}\right) \tag{48}$$

$$\begin{aligned} q^+(\acute{\theta}) &= A\,\omega\cos(\omega\acute{t}) \\ &= A\,\omega\cos\left[\sin^{-1}\left(\frac{\acute{\theta}-\theta_o}{A}\right)\right] \\ &= \omega\sqrt{A^2 - (\acute{\theta}-\theta_o)^2} \end{aligned} \tag{49}$$

$$q^-(\acute{\theta}) = -\omega\sqrt{A^2 - (\acute{\theta}-\theta_o)^2} \tag{50}$$

The corresponding pitch acceleration values are of the same magnitude and sign.

$$\begin{aligned} \dot{q}(\acute{\theta}) &= -A\omega^2\sin(\omega\acute{t}) \\ &= -\omega^2(\acute{\theta}-\theta_o) \end{aligned} \tag{51}$$

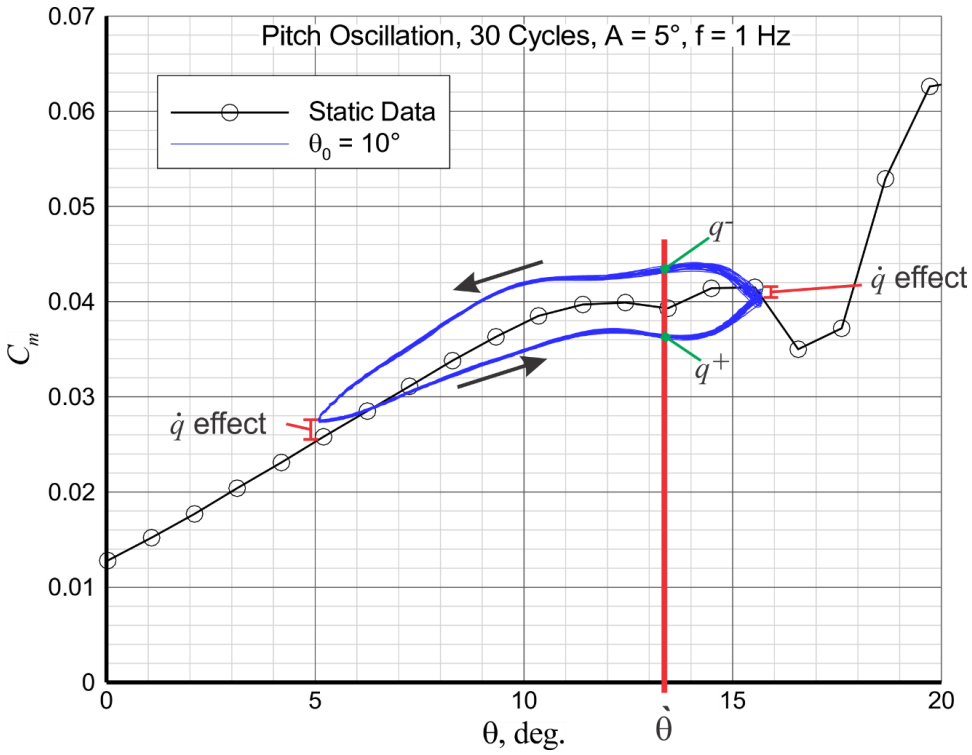

Figure 6 - Pitching moment coefficient hysteresis loop data example from reference 17.

The pitching moment coefficient values at the selected pitch angle $(\acute{\theta})$ can be expressed as:

$$C_m(\acute{\theta}) = C_{m_{\text{static}}}(\acute{\theta}) + \frac{\bar{c}}{2V} q\,(\acute{\theta})\,\overline{C_{m_q}}\,(\acute{\theta}) + \left(\frac{\bar{c}}{2V}\right)^2 \dot{q}(\acute{\theta})\,C_{m_{\dot{q}}}\,(\acute{\theta}) \tag{52}$$

If static data are available from either a conventional pitch-pause sweep or from a very slow rate oscillation (i.e. slow enough that the rate effect is not discernable) then the $C_{m_{\dot{q}}}$ values can be determined from the difference between the oscillation and static values at the oscillation end points where the rate values are zero.

$$\begin{aligned} &\acute{\theta}_{max} = \theta_o + A, \quad \dot{q} = -A\omega^2, \text{and} \quad C_{m_{\dot{q}}}(\acute{\theta}_{max}) = \frac{-1}{A}\left(\frac{2V}{\bar{c}\omega}\right)^2 \left[C_m(\acute{\theta}_{max}) - C_{m_{static}}(\acute{\theta}_{max})\right] \\ &\acute{\theta}_{min} = \theta_o - A, \quad \dot{q} = A\omega^2, \text{ and} \quad C_{m_{\dot{q}}}(\acute{\theta}_{min}) = \frac{1}{A}\left(\frac{2V}{\bar{c}\omega}\right)^2 \left[C_m(\acute{\theta}_{min}) - C_{m_{static}}(\acute{\theta}_{min})\right] \end{aligned} \tag{53}$$

If no static data are available, then the $C_{m_{\dot{q}}}$ values cannot be determined. However, the $\overline{C_{m_q}}$ values can be computed if it is assumed that values are the same for positive and negative rates. This is good assumption for a symmetric airplane oscillating about the roll or yaw body axes. In the pitch axis this may not be true. It should be noted however that this is assumed to be true for both the Integral and Specific Point methods.

If it is assumed that the $\overline{C_{m_q}}$ value is independent of the sign of the rates, then the value is derived in the following manner.

The moment coefficient values at the selected pitch angle $(\acute{\theta})$ with a positive pitch rate can be expressed as:

$$C_m^+(\acute{\theta}) = C_{m_{\text{static}}}(\acute{\theta}) + \frac{\bar{c}}{2V} q^+(\acute{\theta})\,\overline{C_{m_q}}(\acute{\theta}) + \left(\frac{\bar{c}}{2V}\right)^2 \dot{q}(\acute{\theta})\, C_{m_{\dot{q}}}(\acute{\theta}) \tag{54}$$

The negative pitch rate coefficient values are:

$$C_m^-(\acute{\theta}) = C_{m_{\text{static}}}(\acute{\theta}) + \frac{\bar{c}}{2V} q^-(\acute{\theta})\,\overline{C_{m_q}}(\acute{\theta}) + \left(\frac{\bar{c}}{2V}\right)^2 \dot{q}(\acute{\theta})\, C_{m_{\dot{q}}}(\acute{\theta}) \tag{55}$$

The difference between the positive and negative rate coefficient values is:

$$C_m^+(\acute{\theta}) - C_m^-(\acute{\theta}) = \frac{\bar{c}}{2V}\overline{C_{m_q}}(\acute{\theta})\left[q^+(\acute{\theta}) - q^-(\acute{\theta})\right] \tag{56}$$

But $q^+(\acute{\theta}) = -q^-(\acute{\theta})$, so:

$$\overline{C_{m_q}}(\acute{\theta}) = \left(\frac{V}{\bar{c}}\right)\frac{C_m^+(\acute{\theta}) - C_m^-(\acute{\theta})}{q^+(\acute{\theta})} \tag{57}$$

Note that the maximum and minimum pitch acceleration points (where the rate value goes to zero) are singularities.

If the static data are available, then the dynamic coefficients are derived as follows.

Substituting the pitch rate and acceleration equations 49 thru 51 into the positive and negative pitch rate coefficient equations 54 and 55, and subtracting the static values yields:

$$C_m^+(\acute{\theta}) - C_{m_{\text{static}}}(\acute{\theta}) = \left[\frac{\bar{c}\omega}{2V}\sqrt{A^2 - (\acute{\theta} - \theta_o)^2}\right]\overline{C_{m_q}}^+(\acute{\theta}) - \left(\frac{\bar{c}\omega}{2V}\right)^2 (\acute{\theta} - \theta_o)\, C_{m_{\dot{q}}}(\acute{\theta}) \tag{58}$$

$$C_m^-(\acute{\theta}) - C_{m_{\text{static}}}(\acute{\theta}) = \left[-\frac{\bar{c}\omega}{2V}\sqrt{A^2 - (\acute{\theta} - \theta_o)^2}\right]\overline{C_{m_q}}^-(\acute{\theta}) - \left(\frac{\bar{c}\omega}{2V}\right)^2 (\acute{\theta} - \theta_o)\, C_{m_{\dot{q}}}(\acute{\theta}) \tag{59}$$

Solving for the $\overline{C_{m_q}}$ terms yields:

$$\overline{C_{m_q}}^+(\acute{\theta}) = \frac{C_m^+(\acute{\theta}) - C_{m_{\text{static}}}(\acute{\theta}) + \left(\frac{\bar{c}\omega}{2V}\right)^2 (\acute{\theta} - \theta_o)\, C_{m_{\dot{q}}}(\acute{\theta})}{\frac{\bar{c}\omega}{2V}\sqrt{A^2 - (\acute{\theta} - \theta_o)^2}} \tag{60}$$

$$\overline{C_{m_q}}^-(\acute{\theta}) = -\frac{C_m^-(\acute{\theta}) - C_{m_{\text{static}}}(\acute{\theta}) + \left(\frac{\bar{c}\omega}{2V}\right)^2 (\acute{\theta} - \theta_o)\, C_{m_{\dot{q}}}(\acute{\theta})}{\frac{\bar{c}\omega}{2V}\sqrt{A^2 - (\acute{\theta} - \theta_o)^2}} \tag{61}$$

The pitch acceleration coefficient ($C_{m_{\dot{q}}}$) values are only known at the oscillation end points (eq. 53). Therefore, some assumption about the acceleration coefficient values between the end point is required to solve equations 60 and 61 for the $\overline{C_{m_q}}^+$ and $\overline{C_{m_q}}^-$ values. There are two options that will be explored here:

a) Assume $C_{m_{\dot{q}}}$ is linear between the endpoint values

$$C_{m_{\dot{q}}}(\acute{\theta}) = C_{m_{\dot{q}}}(\acute{\theta}_{min}) + \frac{1}{2A}\left[C_{m_{\dot{q}}}(\acute{\theta}_{max}) - C_{m_{\dot{q}}}(\acute{\theta}_{min})\right](\acute{\theta} - \acute{\theta}_{min}) \tag{62}$$

b) Assume $C_{m_{\dot{q}}}$ is one endpoint value for positive accelerations and the other endpoint value for negative accelerations

$$C_{m_{\dot{q}}}(\acute{\theta}) = \begin{cases} C_{m_{\dot{q}}}(\acute{\theta}_{max}) & , \acute{\theta} > \theta_o \\ C_{m_{\dot{q}}}(\acute{\theta}_{min}) & , \acute{\theta} \le \theta_o \end{cases} \tag{63}$$

Applying these two assumptions to the hysteresis loop data shown in figure 6 yields the dynamic coefficient values shown in figure 7. There is a clear difference in the $\overline{C_{m_q}}^{+}$ and $\overline{C_{m_q}}^{-}$ values. However, the choice of the $C_{m_{\dot{q}}}$ interpolation method did not have a large effect on those values.

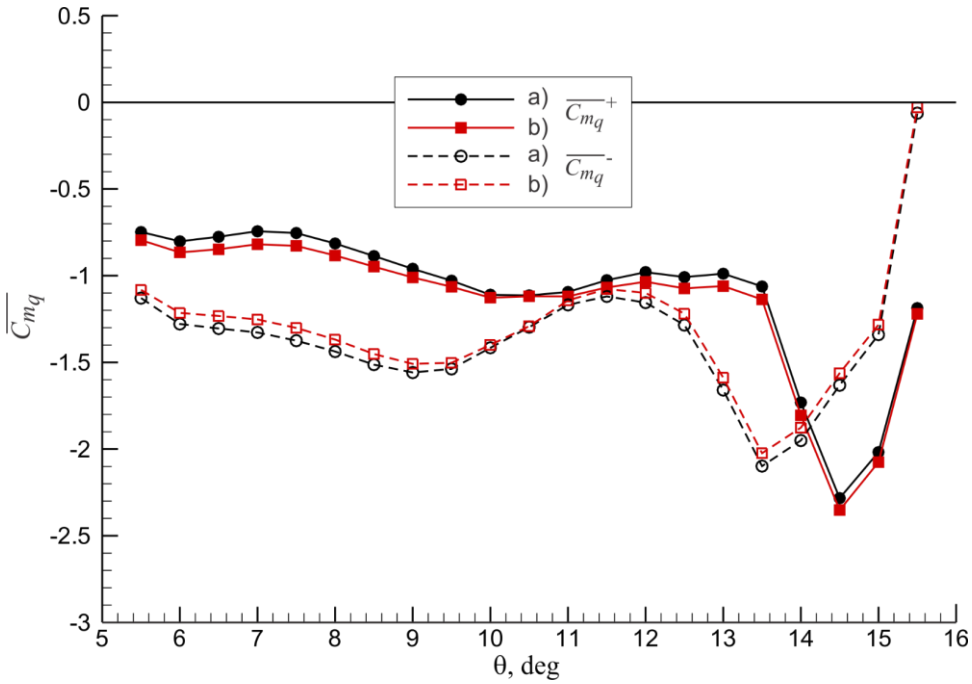

Figure 7 - $\overline{C_{m_q}}$ values computed with different $C_{m_{\dot{q}}}$ assumptions.

A comparison of the Multi-point method $\overline{C_{m_q}}$ results with those from the Specific Point method are presented in figures 8 and 9 for the three oscillation datasets presented previously in figures 4 and 6. These Multi-point results assumed a linear variation of the $C_{m_{\dot{q}}}$ values between the oscillation end points, as shown in figure 10 (a).

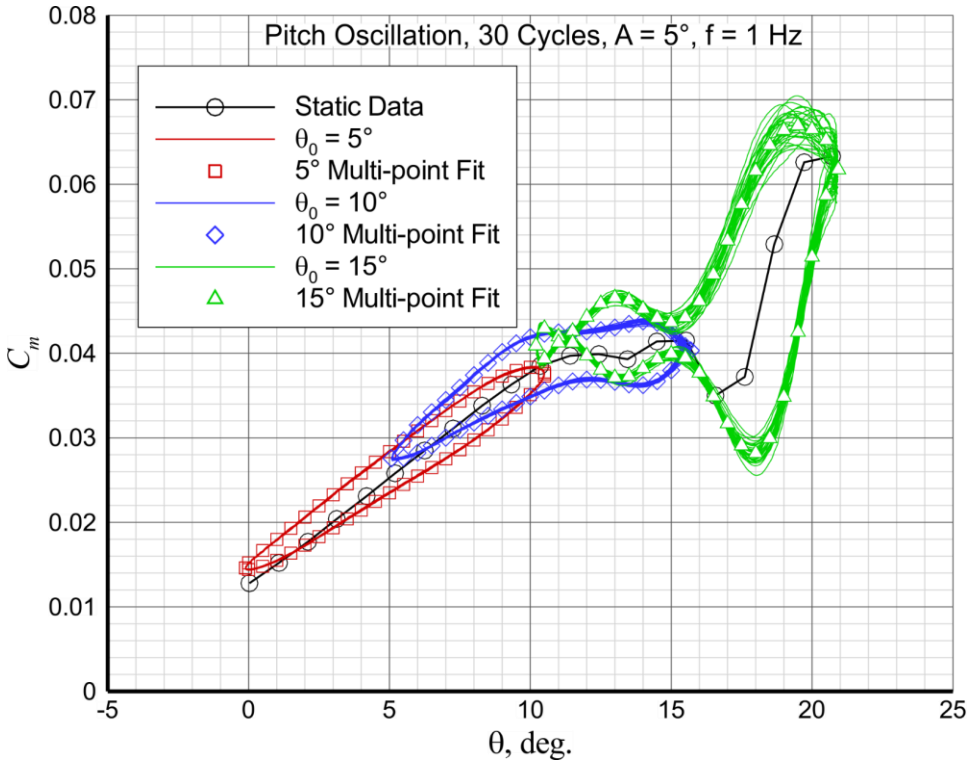

Figure 8 – Multi-point model fit to pitch hysteresis loops.

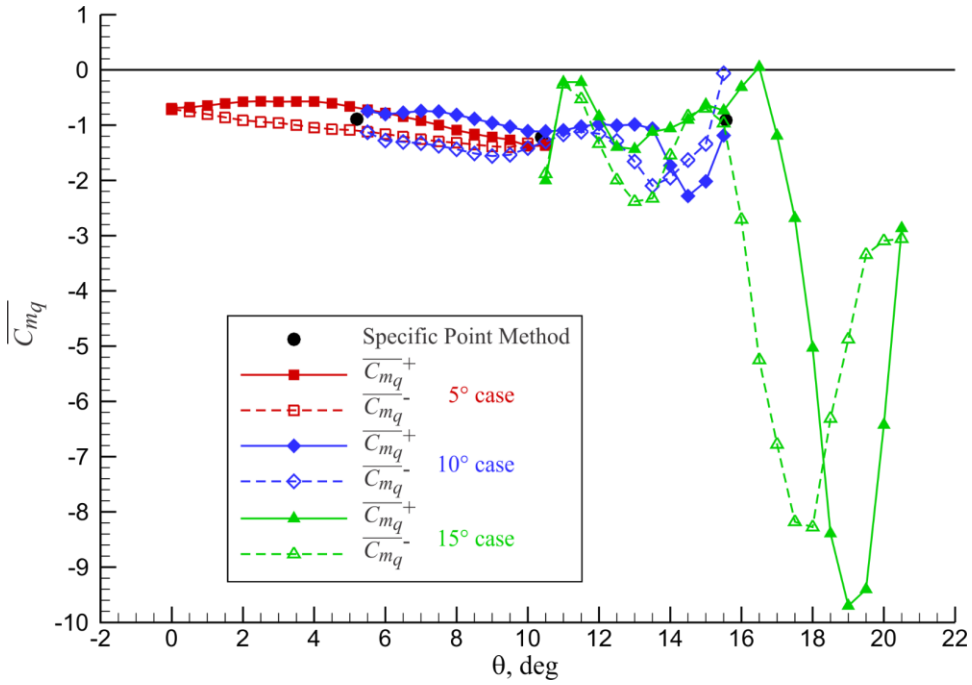

Figure 9 – Multi-point pitch damping coefficient comparison with Specific Point values.

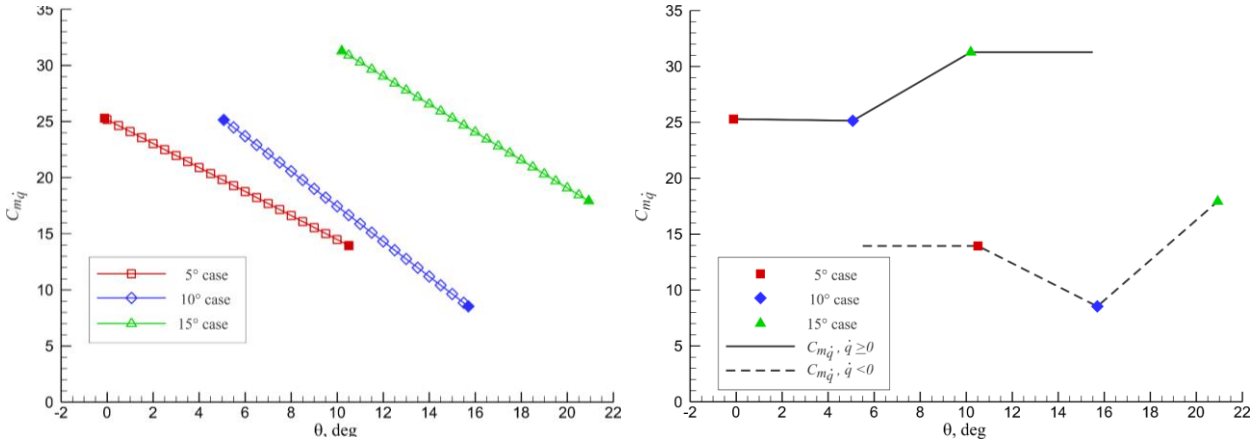

(a) $C_{m_{\dot{q}}}$ linear between the endpoint values. (b) $C_{m_{\dot{q}}}$ a function of the sign of $\dot{q}$.

Figure 10 – Multi-point $C_{m_{\dot{q}}}$ linear model comparison.

As seen in figure 10 (a), the $C_{m_{\dot{q}}}$ end-point values of the three cases don't align or follow a trend. The end-point values were derived from equation 53 and are shown as solid symbols in the figure. This is troubling from a modeling perspective in that the cases overlap in pitch angle and the derived model values ($\overline{C_{m_q}}$, and $C_{m_{\dot{q}}}$) are expected to overlap as well. A possible explanation is that the $C_{m_{\dot{q}}}$ values follow one trend line for positive rates and a different value trend for negative rates, as depicted by the black solid and dashed lines in the figure 10 (b).

Noting that the pitch rate varies throughout the oscillation cycle, the dependence of $\overline{C_{m_q}}$ on the pitch rate can be explored at pitch angles where the oscillation loops overlap. For example, the variation in the $\overline{C_{m_q}}$ values at 8° pitch angle for the 5° and 10° cases of figure 9 are shown in figure 11. Additional pitch rate effects can be explored by varying the amplitude and frequency of the oscillations.

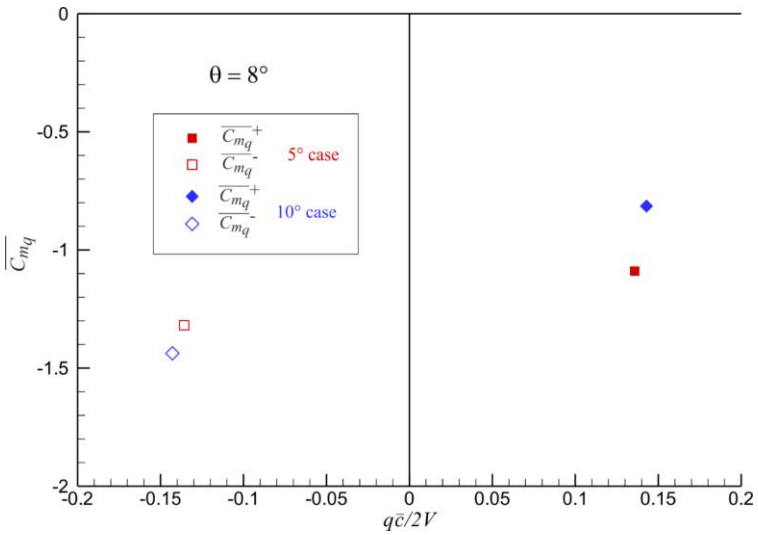

Figure 11 – Multi-point $\overline{C_{m_q}}$ variation with pitch rate at 8° pitch angle.

This Multi-point method looks promising in that it offers greater modeling flexibility and provides a better fit to the non-linear hysteresis loops. However, the method has yet to be used extensively and more experience is required to establish full confidence in this approach.

Data Processing Practical Considerations

Most forced oscillation tests are unique in some way and must be evaluated accordingly. However, there are in general some common considerations and potential error sources (refs. 23-25). The following section will address these areas and provide some best practice suggestions.

Rate Gyro and Position Measurements

The ability to accurately and repeatably reproduce a desired motion (position and rates) with and without wind loads is fundamental to dynamic wind tunnel testing. Not only does the position of the motion have to be accurately measured but that measurement needs to be in phase with the balance measurement. Bergmann, et al. (ref. 26), highlighted several of the important error source considerations for dynamic testing. One of which are the errors associated with balance and position signals being out of sink or phase shifted. Bergmann illustrates this with a $\overline{C_{m_q}}$ measurement example that shows a 2.4% change in coefficient value for each degree of phase shift between the balance and position measurement.

A principal assumption in the method derivations presented earlier in this report is that the test rig forced oscillations are sinusoidal, and as a result, the midpoint of the cycle and the zero-acceleration point are synonymous, and only position information is required. However, in general the test rig motion is not quite a sinusoid and consequently the midpoint of the cycle and the zero-acceleration point may not be the same. Additional instrumentation such as rate gyros or accelerometers will be required to determine the minimum, maximum and zero-acceleration points. The accelerometers or rate gyros signals will likely require some filtering and as noted earlier, any lags in these measurements must be corrected such that the motion and balance measurements are in phase.

Filtering and Cutoff Frequencies

The structural dynamics of the test rig as well as the signal noise of the data acquisition system must be considered with any dynamic forced motion test. The forced motion system must be sufficiently stiff to avoid the structural dynamics contaminating the balance measurements and yet have the flexibility to provide the desired motion. This is generally achieved by limiting the degrees-of-freedom and amplitude of the motion (ref. 27).

A simple ground vibration test of the installed model prior to wind-on testing can provide some insight into the structural dynamics and signal noise. The extent of filtering and cutoff frequencies necessary can then be determined. An example of the effect of a low-pass cutoff filter on the balance signal is provided in reference 16 for a forced oscillation test in the NASA Langley 12-Foot Low-Speed Tunnel and repeated here as figure 12. The figure shows the Fast Fourier Transform results of a raw and filtered balance signal. The filter was a digital Butterworth filter with a cut-off frequency four times the 1Hz oscillation frequency. This 4 Hz low-pass filter clearly diminishes the 8 Hz structural vibration signal. All the data in this example were sampled at 250 Hz with a 50 Hz analog anti-aliasing filter in the data acquisition loop. The sampling rate must be higher than twice the maximum frequency of interest to avoid aliasing (ref. 29).

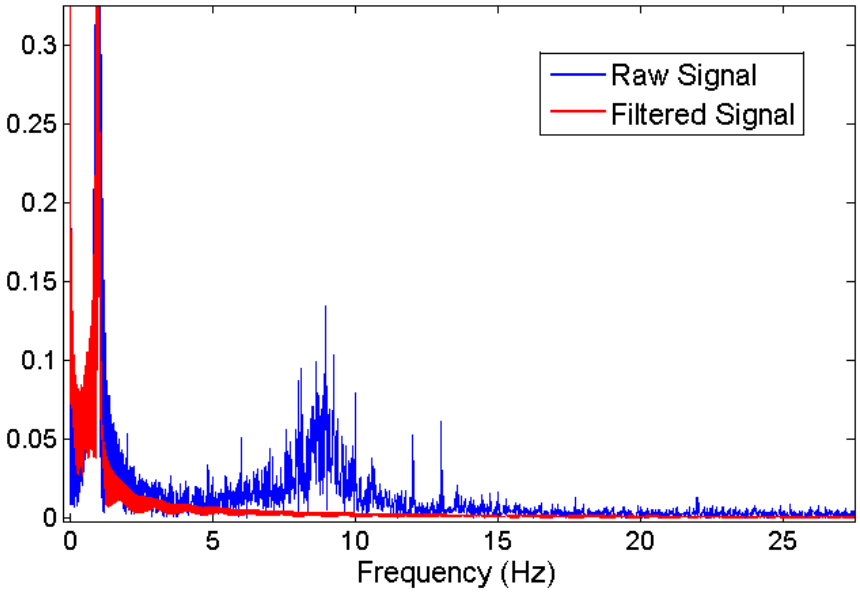

Figure 12 – Example balance signal noise filtering (Figure 11 of AIAA 2012-4645)

Number of Cycles Required

Forced oscillation testing can be a very time-consuming and costly process depending on the frequency and rates being tested. Heim and Brandon (refs. 24, 25) introduce a method to base the number of cycles of data collected on satisfying a set of data accuracy and uncertainty criteria. The common practice was to collect 40 cycles of data, independent of frequency, amplitude, or model attitude (angle of attack and sideslip). Heim and Brandon showed that in the steady linear aerodynamic range significantly fewer cycles could be used and in the unsteady nonlinear range more cycles maybe required. A flowchart of their method is shown in figure 13. The stopping criterion is based on a 10-cycle moving average of the maximum cycle to cycle gradient of the standard deviation (g_m). The maximum gradient indicates how much the uncertainty of the cycle is changing from cycle to cycle. Once the uncertainty stops changing within a given threshold the run is completed.

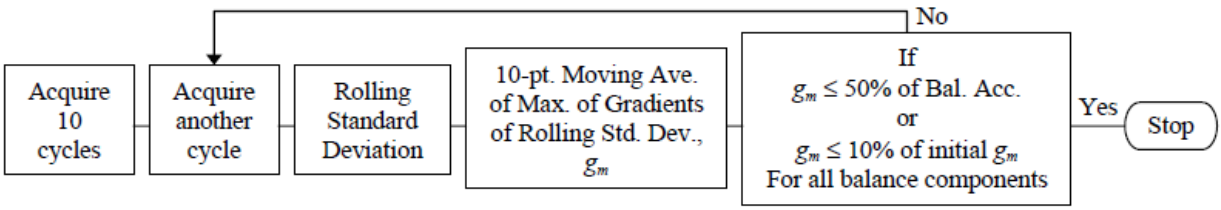

Figure 13 - Flowchart of forced oscillation data acquisition termination process. (Figure 12 of reference 25)

Figure 14 shows an example of the cycles required to meet the terminating condition for yaw oscillations of a fighter model. All the wind-off tares could end after the minimum 11 cycles, as well as the wind-on oscillations at 10° angle of attack. The 38°, 40°, 50° and 60° angle of attack cases required 38, 37, 48 and 40 cycles, respectively.

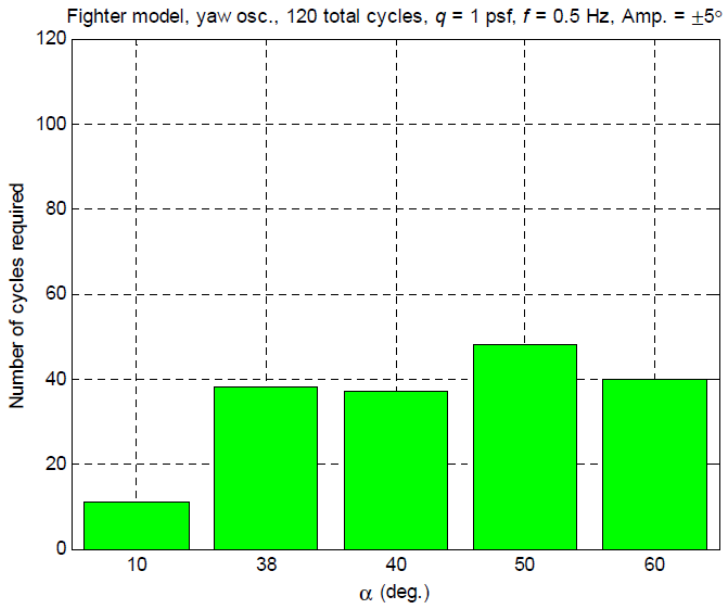

Figure 14 - Cycles required for fighter model using stopping criteria (Figure 13 of reference 25).

Absent any stopping criteria such as that proposed above, the 40-cycle standard appears sufficient. In the non-linear and unsteady aerodynamic regions, it is questionable whether the additional cycles required to acquire a dynamic coefficient value for a linear model that doesn't replicate aerodynamics well, is truly warranted.

Summary

The sinusoidal forced oscillation wind tunnel test technique has been used for many years to measure the dynamic characteristics of both aircraft and spacecraft in the atmosphere. The data processing and analysis used for this test technique has evolved without much supporting documentation. This report has provided some historical background into this evolution along with a derivation of the current data reduction methods and a discussion of their practical application and considerations. This report has described two of the primary methods used to analyze and process the forced oscillation test data and introduced a third. The mathematical derivation of each of these methods is included along with their inherent assumptions and limitations. The report also reviewed some common considerations, limitations and potential error sources of the test technique and provided some best practice suggestions.

References

1.Bird, John D., Jaquet, Byron M., and Cowan, John W. 1951. Effect of Fuselage and Tail Surfaces on Low-Speed Yawing Characteristics of a Swept-Wing Model As Determined in Curved-Flow Test Section of the Langley Stability Tunnel. NACA TN-2483, Langley Field, VA: NACA Langley Aeronautical Laboratory.

2.Campbell, John P., Joseph L. Jr. Johnson, and Donald E. Hewes. 1955. Low-Speed Study of the Effect of Frequency on the Stability Derivatives of Wings Oscillating in Yaw with Particular Reference to High Angle-of-Attack Conditions. NACA RM L55H05, Washington DC: National Advisory Committee for Aeronautics.

3.Chambers, Joseph R. and Grafton, Sue B. 1966. Static and Dynamic Longitudinal Stability Derivatives of a Powered 1/9-scale Model of a Tilt-wing V/STOL Transport. NASA TND-3591, Hampton, VA: NASA Langley Research Center.

4.Chambers, J. R., and S. B. Grafton. Static and dynamic longitudinal stability derivatives of a powered 0.18-scale model of a fan-in-wing VTOL aircraft. No. NASA-TN-D-4322. 1968.

5.Anglin, Ernie L., and J. R. Chambers. Analysis of lateral directional stability characteristics of a twin jet fighter airplane at high angles of attack. No. NASA-TN-D-5361. 1969.

6.Grafton, S. B., and C. E. Libbey. Dynamic stability derivatives of a twin-jet fighter model for angles of attack from-10 deg to 110 deg. No. L-7370. 1971..

7.Grafton, Sue B., Lyle P. Parlett, and Charles C. Smith Jr. Dynamic stability derivatives of a jet transport configuration with high thrust-weight ratio and an externally blown jet flap. No. NASA-TN-D-6440. 1971.

8.Grafton, Sue B., and Ernie L. Anglin. Dynamic stability derivatives at angles of attack from minus 5 deg to 90 deg for a variable-sweep fighter configuration with twin vertical tails. No. L-8426. 1972.

9.Grafton, S. B., M. A. Croom, and L. T. Nguyen. High-angle-of-attack stability characteristics of a 3-surface fighter configuration. No. NASA-TM-84584. 1983.

10. Hahne, David E. Low-speed static and dynamic force tests of a generic supersonic cruise fighter configuration. No. NASA-TM-4138. 1989.

11. Coe Jr, Paul L., Steven G. Turner, and D. Bruce Owens. Low-speed wind-tunnel investigation of the flight dynamic characteristics of an advanced turboprop business/commuter aircraft configuration. No. NASA-TP-2982. 1990.

12. Brandon, Jay, and John Foster. "Recent dynamic measurements and considerations for aerodynamic modeling of fighter airplane configurations." In 23rd Atmospheric Flight Mechanics Conference, p. 4447. 1998..

13. Brandon, Jay, John Foster, Gautam Shah, William Gato, and James Wilborn. "Comparison of rolling moment characteristics during roll oscillations for a low and a high aspect ratio configuration." In AIAA Atmospheric Flight Mechanics Conference and Exhibit, p. 5273. 2004

14. Foster, John, Kevin Cunningham, Charles Fremaux, Gautam Shah, Eric Stewart, Robert Rivers, James Wilborn, and William Gato. "Dynamics modeling and simulation of large transport airplanes in upset conditions." In AIAA Guidance, Navigation, and Control Conference and Exhibit, p. 5933. 2005.

15. Owens, D. Bruce, and Vanessa Aubuchon. "Overview of Orion crew module and launch abort vehicle dynamic stability." In 29th AIAA Applied Aerodynamics Conference, p. 3504. 2011.

16. Hoe, Garrison, D. Bruce Owens, and Casey Denham. "Forced oscillation wind tunnel testing for FASER flight research aircraft." In AIAA Atmospheric Flight Mechanics Conference, p. 4645. 2012.

17. Vicroy, Dan D., Thomas D. Loeser, and Andreas Schütte. 2012. "Static and Forced-Oscillation Tests of a Generic Unmanned Combat Air Vehicle." Journal of Aircraft (American Institute of Aeronautics and Astronautics) 49 (6): 1558-1583. doi: 10.2514/1.C031501.

18. Aubuchon, Vanessa V., D. Bruce Owens, Olman Carvajal, and Stewart B. Lumb. "Dynamic stability of the Boeing CST-100." In AIAA Atmospheric Flight Mechanics Conference, p. 1399. 2017.

19. Cunningham, Kevin, Gautam H. Shah, Neal T. Frink, Susan N. McMillin, Patrick C. Murphy, Frank R. Brown, Patrick J. Hayes, Kamal M. Shweyk, and Sudheer N. Nayani. "Preliminary test results for stability and control characteristics of a generic T-tail transport airplane at high angle of attack." In 2018 AIAA Atmospheric Flight Mechanics Conference, p. 0529. 2018.

20. Hultberg, Randy S. 1998. "Acquisition Technique and Analysis Format for Forced Oscillation Dynamic Data." High-Angle-of-Attack Technology: Accomplishments, Lessons Learned and Future Directions. Hampton, VA: NASA/CP-1998-207676. pp 707-743.

21. Hunsaker, Jerome C. “Report on Behavior of Aeroplanes in Gusts. Part I. Experimental Analysis of Inherent Longitudinal Stability for a Typical Biplane.” NACA TR-1, 1917.

22. Coleman, Hugh W. and Steele, W. Glenn. 1999, 2nd ed. Experimentation and Uncertainty Analysis for Engineers. New York: John Wiley & Sons, Inc.

23. Bergmann, Andreas, Andreas Huebner, and Thomas Loeser. 2008. "Experimental and numerical research on the aerodynamics of unsteady moving aircraft." Progress in Aerospace Sciences, 121-137. https://doi.org/10.1016/j.paerosci.2007.10.006.

24. Heim, Eugene Henry DeWendt. "Development of methods for improved data integrity and efficient testing of wind tunnel models for dynamic test conditions in unsteady and nonlinear flight regimes." MS thesis, Virginia Tech, 2003.

25. Heim, Eugene H. D., and Jay M. Brandon. 2004. Uncertainty-Based Approach for Dynamic Aerodynamic Data Acquisition and Analysis. AIAA 2004-5364, AIAA.

26. Bergmann, Andreas, Thomas Loeser, and Andreas Huebner. 2011. "Improvement of Ground Test Facilities for Dynamic Testing - Survey from the Past up to Now." NATO RTO-MP-AVT-189 Assessment of Stability and Control Prediction Methods for NATO Air and Sea Vehicles.

27. Bergmann, A. 2009. Modern Wind Tunnel Techniques for Unsteady Testing – Development of Dynamic Test Rigs. Vol. 102, in Hermann Schlichting – 100 Years. Notes on Numerical Fluid Mechanics and Multidisciplinary Design, by Rossow CC., Brinkmann B.W. (eds) Radespiel R., 55-77. Berlin, Heidelberg: Springer. https://doi.org/10.1007/978-3-540-95998-4_5.

28 Smith, David L. 1972. An Efficient Algorithm Using Matrix Methods to Solve Wind-Tunnel Force-Balance Equations. NASA TND-6860, Hampton, VA: NASA Langley Research Center.

29. Hardin, Jay C. 1990. Introduction to Time Series Analysis. NASA RP-1145, NASA Langley Research Center, Washington, DC: National Aeronautics and Space Administration.

Appendix

Integration Method Coefficient Equations

Roll Axis Coefficients

The body roll axis forced oscillation coefficient values are:

Force coefficients:

$$C_{a_0}(\alpha_o,\beta_o) = \frac{1}{\bar{q}ST}\int_{t_0}^{t_0+T}\left[F_{a_b}(t) - F_{a_i}(t)\right]dt\ ,\ a = A,Y,N \tag{64}$$

$$\overline{C_{a_\beta}}(\alpha_o,\beta_o) = \frac{2}{\bar{q}SAT}\int_{t_0}^{t_0+T}\left[F_{a_b}(t) - F_{a_i}(t)\right]\sin(\omega t)\,dt\ ,\ a = A,Y,N \tag{65}$$

$$\overline{C_{a_p}}(\alpha_o,\beta_o) = \frac{4V}{\bar{q}Sb\omega AT}\int_{t_0}^{t_0+T}\left[F_{a_b}(t) - F_{a_i}(t)\right]\cos(\omega t)\,dt\ ,\ a = A,Y,N \tag{66}$$

Moment coefficients:

$$C_{l_0}(\alpha_o,\beta_o) = \frac{1}{\bar{q}SbT}\int_{t_0}^{t_0+T}[L_b(t) - L_i(t)]\,dt \tag{67}$$

$$\overline{C_{l_\beta}}(\alpha_o,\beta_o) = C_{l_\beta}\sin\alpha - \left(\frac{\omega b}{2V}\right)^2 C_{l_{\dot{p}}} = \frac{2}{\bar{q}SbAT}\int_{t_0}^{t_0+T}[L_b(t) - L_i(t)]\sin(\omega t)\,dt \tag{68}$$

$$\overline{C_{l_p}}(\alpha_o,\beta_o) = C_{l_p} + C_{l_{\dot{\beta}}}\sin\alpha = \frac{4V}{\bar{q}Sb^2\omega AT}\int_{t_0}^{t_0+T}[L_b(t) - L_i(t)]\cos(\omega t)\,dt \tag{69}$$

$$C_{m_0}(\alpha_o,\beta_o) = \frac{1}{\bar{q}S\bar{c}T}\int_{t_0}^{t_0+T}[M_b(t) - M_i(t)]\,dt \tag{70}$$

$$\overline{C_{m_\beta}}(\alpha_o,\beta_o) = \frac{2}{\bar{q}S\bar{c}AT}\int_{t_0}^{t_0+T}[M_b(t) - M_i(t)]\sin(\omega t)\,dt \tag{71}$$

$$\overline{C_{m_p}}(\alpha_o,\beta_o) = \frac{4V}{\bar{q}S\bar{c}b\omega AT}\int_{t_0}^{t_0+T}[M_b(t) - M_i(t)]\cos(\omega t)\,dt \tag{72}$$

$$C_{n_0}(\alpha_o,\beta_o) = \frac{1}{\bar{q}SbT}\int_{t_0}^{t_0+T}[N_b(t) - N_i(t)]\,dt \tag{73}$$

$$\overline{C_{n_\beta}}(\alpha_o,\beta_o) = \frac{2}{\bar{q}SbAT}\int_{t_0}^{t_0+T}[N_b(t) - N_i(t)]\sin(\omega t)\,dt \tag{74}$$

$$\overline{C_{n_p}}(\alpha_o,\beta_o) = \frac{4V}{\bar{q}Sb^2\omega AT}\int_{t_0}^{t_0+T}[N_b(t) - N_i(t)]\cos(\omega t)\,dt \tag{75}$$

Pitch Oscillation Coefficients

The body pitch axis forced oscillation coefficient values are:

Force coefficients:

$$C_{a_0}(\alpha_o,\beta_o) = \frac{1}{\bar{q}ST}\int_{t_0}^{t_0+T}\left[F_{a_b}(t) - F_{a_i}(t)\right]dt\ ,\ a = A,Y,N \tag{76}$$

$$\overline{C_{a_\alpha}}(\alpha_o,\beta_o) = \frac{2}{\bar{q}SAT}\int_{t_0}^{t_0+T}\left[F_{a_b}(t) - F_{a_i}(t)\right]\sin(\omega t)\,dt\ ,\ a = A,Y,N \tag{77}$$

$$\overline{C_{a_q}}(\alpha_o,\beta_o) = \frac{4V}{\bar{q}S\bar{c}\omega AT}\int_{t_0}^{t_0+T}\left[F_{a_b}(t) - F_{a_i}(t)\right]\cos(\omega t)\,dt\ ,\ a = A,Y,N \tag{78}$$

Moment coefficients:

$$C_{l_0}(\alpha_o,\beta_o) = \frac{1}{\bar{q}SbT}\int_{t_0}^{t_0+T}[L_b(t) - L_i(t)]\,dt \tag{79}$$

$$\overline{C_{l_\alpha}}(\alpha_o,\beta_o) = \frac{2}{\bar{q}SbAT}\int_{t_0}^{t_0+T}[L_b(t) - L_i(t)]\sin(\omega t)\,dt \tag{80}$$

$$\overline{C_{l_q}}(\alpha_o,\beta_o) = \frac{4V}{\bar{q}S\bar{c}b\omega AT}\int_{t_0}^{t_0+T}[L_b(t) - L_i(t)]\cos(\omega t)\,dt \tag{81}$$

$$C_{m_0}(\alpha_o,\beta_o) = \frac{1}{\bar{q}S\bar{c}T}\int_{t_0}^{t_0+T}[M_b(t) - M_i(t)]\,dt \tag{82}$$

$$\overline{C_{m_\alpha}}(\alpha_o,\beta_o) = C_{m_\alpha} - \left(\frac{\bar{c}\omega}{2V}\right)^2 C_{m_{\dot{q}}} = \frac{2}{\bar{q}S\bar{c}AT}\int_{t_0}^{t_0+T}[M_b(t) - M_i(t)]\sin(\omega t)\,dt \tag{83}$$

$$\overline{C_{m_q}}(\alpha_o,\beta_o) = C_{m_q} - C_{m_{\dot{\alpha}}} = \frac{4V}{\bar{q}S\bar{c}^2\omega AT}\int_{t_0}^{t_0+T}[M_b(t) - M_i(t)]\cos(\omega t)\,dt \tag{84}$$

$$C_{n_0}(\alpha_o,\beta_o) = \frac{1}{\bar{q}SbT}\int_{t_0}^{t_0+T}[N_b(t) - N_i(t)]\,dt \tag{85}$$

$$\overline{C_{n_\alpha}}(\alpha_o,\beta_o) = \frac{2}{\bar{q}SbAT}\int_{t_0}^{t_0+T}[N_b(t) - N_i(t)]\sin(\omega t)\,dt \tag{86}$$

$$\overline{C_{n_q}}(\alpha_o,\beta_o) = \frac{4V}{\bar{q}S\bar{c}b\omega AT}\int_{t_0}^{t_0+T}[N_b(t) - N_i(t)]\cos(\omega t)\,dt \tag{87}$$

Yaw Axis Coefficients

The body yaw axis forced oscillation coefficient values are:

Force coefficients:

$$C_{a_0}(\alpha_o,\beta_o) = \frac{1}{\bar{q}ST}\int_{t_0}^{t_0+T}\left[F_{a_b}(t) - F_{a_i}(t)\right]dt\ ,\ a = A,Y,N \tag{88}$$

$$\overline{C_{a_\beta}}(\alpha_o,\beta_o) = \frac{2}{\bar{q}SAT}\int_{t_0}^{t_0+T}\left[F_{a_b}(t) - F_{a_i}(t)\right]\sin(\omega t)\,dt\ ,\ a = A,Y,N \tag{89}$$

$$\overline{C_{a_r}}(\alpha_o,\beta_o) = \frac{4V}{\bar{q}Sb\omega AT}\int_{t_0}^{t_0+T}\left[F_{a_b}(t) - F_{a_i}(t)\right]\cos(\omega t)\,dt\ ,\ a = A,Y,N \tag{90}$$

Moment coefficients:

$$C_{l_0}(\alpha_o,\beta_o) = \frac{1}{\bar{q}SbT}\int_{t_0}^{t_0+T}[L_b(t) - L_i(t)]\,dt \tag{91}$$

$$\overline{C_{l_\beta}}(\alpha_o,\beta_o) = \frac{2}{\bar{q}SbAT}\int_{t_0}^{t_0+T}[L_b(t) - L_i(t)]\sin(\omega t)\,dt \tag{92}$$

$$\overline{C_{l_r}}(\alpha_o,\beta_o) = \frac{4V}{\bar{q}Sb^2\omega AT}\int_{t_0}^{t_0+T}[L_b(t) - L_i(t)]\cos(\omega t)\,dt \tag{93}$$

$$C_{m_0}(\alpha_o,\beta_o) = \frac{1}{\bar{q}S\bar{c}T}\int_{t_0}^{t_0+T}[M_b(t) - M_i(t)]\,dt \tag{94}$$

$$\overline{C_{m_\beta}}(\alpha_o,\beta_o) = \frac{2}{\bar{q}S\bar{c}AT}\int_{t_0}^{t_0+T}[M_b(t) - M_i(t)]\sin(\omega t)\,dt \tag{95}$$

$$\overline{C_{m_r}}(\alpha_o,\beta_o) = \frac{4V}{\bar{q}S\bar{c}b\omega AT}\int_{t_0}^{t_0+T}[M_b(t) - M_i(t)]\cos(\omega t)\,dt \tag{96}$$

$$C_{n_0}(\alpha_o,\beta_o) = \frac{1}{\bar{q}SbT}\int_{t_0}^{t_0+T}[N_b(t) - N_i(t)]\,dt \tag{97}$$

$$\overline{C_{n_\beta}}(\alpha_o,\beta_o) = C_{n_\beta}\cos\alpha + \left(\frac{\omega b}{2V}\right)^2 C_{n_{\dot{r}}} = \frac{2}{\bar{q}SbAT}\int_{t_0}^{t_0+T}[N_b(t) - N_i(t)]\sin(\omega t)\,dt \tag{98}$$

$$\overline{C_{n_r}}(\alpha_o,\beta_o) = C_{n_r} - C_{n_{\dot{\beta}}}\cos\alpha = \frac{4V}{\bar{q}Sb^2\omega AT}\int_{t_0}^{t_0+T}[N_b(t) - N_i(t)]\cos(\omega t)\,dt \tag{99}$$

Specific Point Method Coefficient Equations

Roll Axis Coefficients

$$C_{a_o} = \frac{1}{2}[C_a(p_{max}) + C_a(p_{min})]\ ,\ a = A, Y, N, l, m, n \tag{100}$$

$$\overline{C_{a_\beta}} = \frac{-1}{2A}[C_a(\dot{p}_{max}) - C_a(\dot{p}_{min})]\ ,\ a = A, Y, N, l, m, n \tag{101}$$

$$\overline{C_{a_p}} = \frac{V}{bA\omega}[C_a(p_{max}) - C_a(p_{min})]\ ,\ a = A, Y, N, l, m, n \tag{102}$$

Pitch Axis Coefficients

$$C_{a_o} = \frac{1}{2}[C_a(q_{max}) + C_a(q_{min})]\ ,\ a = A, Y, N, l, m, n \tag{103}$$

$$\overline{C_{a_\alpha}} = \frac{-1}{2A}[C_a(\dot{q}_{max}) - C_a(\dot{q}_{min})]\ ,\ a = A, Y, N, l, m, n \tag{104}$$

$$\overline{C_{a_q}} = \frac{V}{\bar{c}A\omega}[C_a(q_{max}) - C_a(q_{min})]\ ,\ a = A, Y, N, l, m, n \tag{105}$$

Yaw Axis Coefficients

$$C_{a_o} = \frac{1}{2}[C_a(r_{max}) + C_a(r_{min})]\ ,\ a = A, Y, N, l, m, n \tag{106}$$

$$\overline{C_{a_\beta}} = \frac{-1}{2A}[C_a(\dot{r}_{max}) - C_a(\dot{r}_{min})]\ ,\ a = A, Y, N, l, m, n \tag{107}$$

$$\overline{C_{a_r}} = \frac{V}{bA\omega}[C_a(r_{max}) - C_a(r_{min})]\ ,\ a = A, Y, N, l, m, n \tag{108}$$

Specific Point Method Implementation

The following is a step-by-step description of the forced-oscillation data processing for the Specific Point method.

1) **Process the wind-off tare time history data.**
   The first step in the forced-oscillation data analysis is processing the wind-off tare data. Most of these wind-off tare processing steps will be replicated for the wind-on data processing.
   a. The balance voltage time history measurements are processed into engineering units using the balance calibration equations. (ref. 28)
   b. It is often desired to delete a set number of time history data points at the beginning and end of the oscillation to exclude any transients resulting from the start and stop motions. The default number of points is 100.
   c. The average sample time increment is determined from the first and last sample time divided by one less than the number of data points (n).
   $$\Delta t = \frac{t(n) - t(1)}{n - 1}$$
   d. The balance and position measurements are passed through a digital low-pass filter to remove unwanted signal or structural noise. The default low-pass frequency limit is 5Hz. Both the position

and balance measurements should be passed through the filter so all will have the same filter phase shift if any.

e. The amplitude of the oscillation is computed from the filtered position signal as half the difference between the maximum and minimum values.

$$A = \frac{1}{2}(\theta_{\max} - \theta_{\min})$$

f. The nominal position signal is computed as the average of the maximum and minimum values.

$$\theta_o = \frac{1}{2}(\theta_{\max} + \theta_{\min})$$

g. A SIN signal is generated from position, amplitude and nominal values.

$$\mathrm{SIN}(t) = \frac{(\theta(t) - \theta_o)}{A}$$

h. The next step is collecting the balance measurements at maximum and minimum rate points and the maximum and minimum acceleration points. The maximum rate occurs at the positive slope zero crossings of the SIN signal. The indices of the SIN signal at or just prior to these zero crossings can be obtained with the Matlab command:

```
ixspos = find((SIN(1:end-1).* SIN(2:end) < 0 &...
         gradient(SIN(1:end-1)) > 0) | (SIN(1:end-1) == 0 &...
         gradient(SIN(1:end-1)) > 0) )
```

i. The positive rate crossing times are determined by linear interpolation of the TIME and SIN signals across the increment segment.

$$t_{x+}(i_{xs+}) = \mathrm{TIME}(i_{xs+}) - \mathrm{SIN}(i_{xs+})\frac{\mathrm{TIME}(i_{xs+}+1) - \mathrm{TIME}(i_{xs+}+1)}{\mathrm{SIN}(i_{xs+}+1) - \mathrm{SIN}(i_{xs+})}$$

j. The zero crossings indices corresponding to the minimum rate of the oscillation cycle are obtained in a similar manner. The of the SIN signal at or just prior to zero crossing with a negative slope can be found with the Matlab command:

```
ixsneg = find((SIN(1:end-1).*SIN(2:end) < 0 &...
         gradient(SIN(1:end-1)) < 0) | (SIN(1:end-1) == 0 &...
         gradient(SIN(1:end-1)) < 0) )
```

k. The minimum rate crossing times are determined by linear interpolation of the TIME and SIN signals similar to step (i).

$$t_{x-}(i_{xs-}) = \mathrm{TIME}(i_{xs-}) - \mathrm{SIN}(i_{xs-})\frac{\mathrm{TIME}(i_{xs-}+1) - \mathrm{TIME}(i_{xs-}+1)}{\mathrm{SIN}(i_{xs-}+1) - \mathrm{SIN}(i_{xs-})}$$

l. The positive rate crossing times are used to compute the average period and frequency.

$$t_{period} = \frac{t_{x+}(nx_+) - t_{x+}(1)}{nx_+ - 1}$$

where nx_+ is the number of positive rate crossing points.

$$f = \frac{1}{t_{period}}$$

m. A COS signal is created to extract the maximum and minimum acceleration points.

   i. Create radians values for each positive rate crossing time.

   $$r_{x+}(i) = 2\pi(i-1) \quad , i = 1,2,3, \ldots\ nx_+$$

   ii. Linear interpolate a radians value $r(t)$ for each TIME value using the crossing time $t_{x+}(i)$ and corresponding radians values $r_{x+}(i)$.

   iii. Compute a COS signal from the interpolated radians values.

   $$\mathrm{COS}(t) = \cos\big(r(t)\big)$$

n. Find the positive and negative rate crossing indices and times of the COS signal in the same manner as steps (h) thru (k). These values correspond to the minimum and maximum acceleration crossing values, respectively.

```
ixcpos = find((COS(1:end-1).*COS(2:end) < 0 &...
         gradient(COS(1:end-1)) > 0) | (COS(1:end-1) == 0 &...
         gradient(COS(1:end-1)) > 0) )

ixcneg = find((COS(1:end-1).*COS(2:end) < 0 &...
         gradient(COS(1:end-1)) < 0) | (COS(1:end-1) == 0 &...
         gradient(COS(1:end-1)) < 0) )
```

o. Linearly interpolate the balance time history values at the minimum and maximum rate and acceleration crossing times.
p. Compute the mean and standard deviation of the balance crossing values.
q. Store the crossing values as well as their mean and standard deviation values.

2) **Process the wind-on time history data and compute dynamic derivatives.**
   a. Repeat steps (1a) thru (1q) with the wind-on time history data.
   b. Subtract the mean crossing values of the tare from the wind-on values for each balance signal.
   c. Non-dimensionalize these balance deltas into coefficient form.
   d. Non-dimensionalize these balance crossing standard deviations into coefficient form.
   e. Compute the dynamic derivative values. (eqs 27, 29 and 35).
   f. Compute the dynamic derivative standard deviation values (eq. 41).
   g. Store the dynamic derivatives and their standard deviation values